Nano-scale TEM Studies of the Passive Film and Chloride-induced Depassivation of Carbon Steel in Concrete

P. Ghods[*], O. B. Isgor[**], J. Li[***], G. J. C. Carpenter[****], G. McRae[*****] and G. P. Gu[******]

[*] Carleton University, Ottawa, ON, Canada, pghods@connect.carleton.ca
[**] Carleton University, Ottawa, ON, Canada, oisgor@carleton.ca
[***] CANMET Materials Technology Laboratories, Ottawa, ON, Canada, jili@nrcan.gc.ca
[****] CANMET Materials Technology Laboratories, Ottawa, ON, Canada, gcarpent@nrcan.gc.ca
[*****] Carleton University, Ottawa, ON, Canada, gmcrae@mae.carleton.ca
[******] CANMET Materials Technology Laboratories, Ottawa, ON, Canada, ggu@nrcan.gc.ca

ABSTRACT

In the highly alkaline environment of concrete, carbon steel rebar is protected against corrosion by a passive iron oxide film. The partial or complete loss of the protective oxide film, known as depassivation, leads to increased rates of rebar corrosion. Understanding the compositional and morphological characteristics of the passive film on rebar, and how it depassivates, is key to mitigate problems associated with corrosion of rebar in concrete. In this study, nano-scale TEM techniques have been used to characterize the passive films on carbon steel in surrogate concrete pore solutions. In chloride-free solutions, oxide films on the samples had a relatively uniform thickness that ranged from 5 to 8 nm, however, after exposure to chloride in amounts greater than typical depassivation thresholds, the thickness of the films became more variable and thinner on average. TEM dark-field images showed the oxide to be comprised of crystalline nano-particles with widths less than 8 nm.

Keywords: TEM, passive film, steel rebar, corrosion, chloride.

1 INTRODUCTION

Understanding the depassivation mechanism of carbon steel rebar in concrete due to chloride attack is key to the development of methods to mitigate problems associated with chloride-induced corrosion initiation in reinforced concrete structures. Although a number of researchers have proposed general mechanistic models [1-3], they do not explain experimental observations regarding the depassivation of carbon steel in highly alkaline environments such as concrete pore solution; therefore, additional studies are needed.

The investigation of passive films and depassivation processes is challenging and requires the use of nano-scale techniques. So far, only a few studies using some of these techniques have been carried out to study iron or steel passivity in highly alkaline environments [4-7]; and, to our knowledge, transmission electron microscopy (TEM) has not been used to investigate the passivity and depassivation of carbon steel in concrete pore solutions.

In this study, (bright-field and dark-field) TEM imaging and energy-dispersive X-ray spectroscopy (EDS) were used as nano-scale techniques to study the passive films on carbon steel that were grown in saturated calcium hydroxide (CH) solution.

2 EXPERIMENTAL SETUP

2.1 Preparation of specimens

TEM samples were made from the cross sections of 10 mm long rebar specimens cut from as-received deformed carbon steel rebar with 10 mm nominal diameter. The chemical composition of the steel is given in Table 1. Two rebar samples were mounted in low-shrinkage epoxy under vacuum. The cross sections of each cold-mounted specimen (see Fig. 1) was subsequently ground and polished using water-free polishing media and finished with 1 μm diamond suspension. After polishing, all cold-mounted specimens were kept in anhydrous alcohol, to avoid exposure to air, until they were transferred to the beakers containing CH solution (pH 12.5) where the passive films were formed on the cross sections of the rebar specimens. The CH solution was prepared by dissolving analytical grade calcium hydroxide in distilled water. The specimens were kept in the solutions for 15 days to allow the formation of stable passive films on the cross sections [8]. After passivation, one specimen was taken out from the solution; this specimen (CH-0) was used to investigate the passive films before exposure to chlorides. Following this, chloride was added to 0.45 M, which is beyond typical chloride thresholds [9]. After two weeks of immersion, the second specimen (CH-Cl) was taken out of the solution.

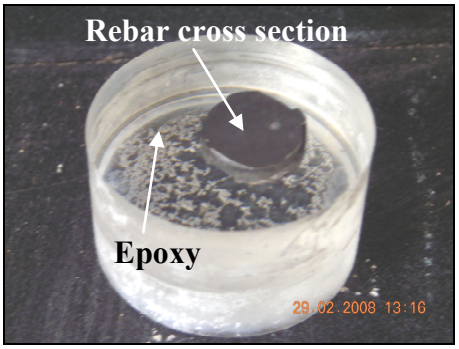

Figure 1: A cold-mounted rebar specimen that was used in the FIB-TEM study.

Element	Weight %
C	0.26
Si	0.27
Mn	1.10
Cr	0.05
Ni	0.07
Mo	<0.01
Cu	0.21
Al	<0.005
Nb	<0.01
V	<0.005
Ti	<0.005
B	<0.0005
P	0.01
S	0.03
W	<0.01
Sn	0.021
Co	0.01
Zr	<0.01
Fe	Balance

Table 1: Elemental composition of the rebar used in the TEM investigation

2.2 FIB sampling

Each specimen was transferred to the focused ion beam (FIB) microscope. A layer of tungsten (W) was sputtered on a ~200 μm by ~50 μm area of interest on the gold-covered cross section of the rebar specimen. The FIB H-bar lift-out method was used to extract the TEM sample from the gold and tungsten covered cross section of the rebar specimen. A gallium ion beam was used to make two trenches on the surface of the specimen. The edges of the area between the two trenches were then cut in order to release the sample from the bulk material. The released sample was placed on a copper TEM grid using a micro-manipulator. The middle part of the sample was milled to ~100 nm thickness using a gallium ion beam (Fig. 2) so that it was electron transparent.

2.3 TEM microscopy

The prepared TEM samples were examined in a transmission electron microscope (TEM) (Model: Philips CM20FEG) equipped with a Schottky field emission gun operated at 200 kV. Conventional bright-field TEM imaging was used to visualize the passive film. Dark-field TEM imaging was also used to determine the amorphous and crystalline phases. Chemical analysis was performed using a thin-window EDS detector from Oxford Instruments equipped with an INCA system analyzer. EDS analyses were obtained in scanning transmission electron microscopy (STEM) mode using a probe diameter of 1~2 nm.

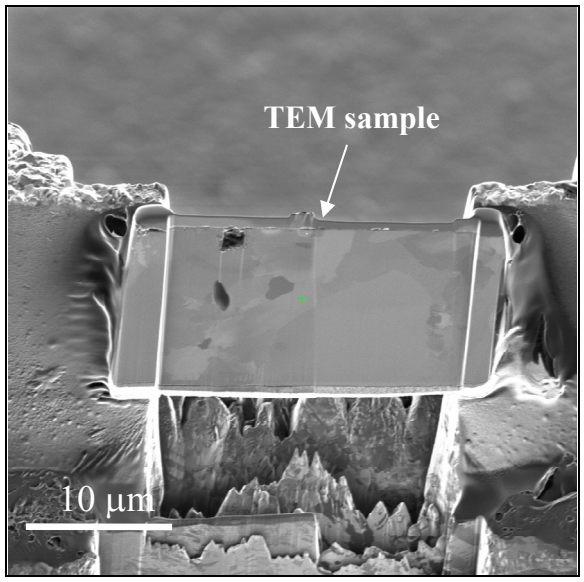

Figure 2: Process of thinning the TEM sample in the FIB microscope using the Gallium ion beam

3 RESULTS AND DISCUSSIONS

TEM micrograph of the CH-0 sample exposed to chloride-free CH passivating solution is shown in Fig. 3. A thin oxide film between the steel substrate and the gold layer is visible in the micrograph image. The oxide film has relatively uniform thickness. From this image, it is difficult to extract a good estimate of the thickness of the film, mainly due to the fact that the TEM samples were approximately 100 nm thick, and the layer that is visible in Fig. 3 represents the two dimensional projection of the oxide films across the depth of the TEM samples. Therefore, it is expected that the oxide film is thinner than the thickest part of the film in the TEM micrographs given in Fig. 3. The thickness of the oxide film can be estimated to range from 5 to 8 nm.

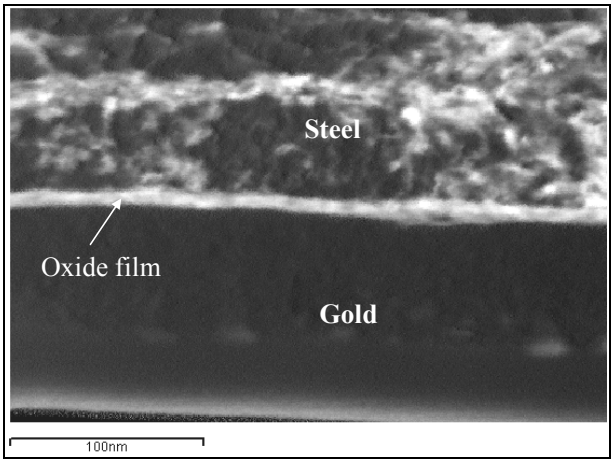

Figure 3: An TEM image of the CH-0 sample passivated in chloride-free solution (the oxide film thickness: 5 to 8 nm).

EDS analysis was carried out to investigate the elemental composition of the oxide films. Typical EDS spectrum obtained at the midpoint of oxide films grown in the CH solution is presented in Fig. 4. EDS analyses of different locations along the oxide film provided similar spectra. Oxygen and iron peaks in the spectra are the indication of the presence of iron oxides. Trace amounts of manganese, silicon and carbon in the EDS spectra originate from the steel substrate. Calcium was also detected in the spectra; this can be attributed to the presence of calcium in the structure of oxide film.

EDS analyses across the width of the oxide films provided information on the film composition with thickness. Results for the oxide film on the CH-0 sample are presented in Fig.5. Figure 5(a) shows the line along which EDS spectra were measured. Figure 5(b) shows the relative atomic percentages of the major elements along the line. The ratio of iron-to-oxygen decreases in the direction of the free surface (i.e., Gold layer).

TEM micrographs of the CH-Cl sample, which was exposed to the CH solution plus 0.45 M chloride, are shown in Fig. 6. Figure 6(a) shows that the thickness of the oxide film on the CH-Cl sample is thinner and more variable when compared with the thicker films on the CH-0 samples (see Fig. 3). On average, the thickness of the film on the CH-Cl samples is ~3 nm, and ranges between 2 nm and 10 nm, whereas the CH-0 films are more uniform and in the range of 5-8 nm, as described previously. Fig. 6(b) shows part of the oxide film where the thickness is < ~3 nm.

Further examination of the CH-Cl sample also showed the presence of pits, with depths ranging from 30 nm to 100 nm, on the steel surface. In Fig. 7, two pits are shown on the surface of the CH-Cl sample on which the oxide film is partially destroyed.

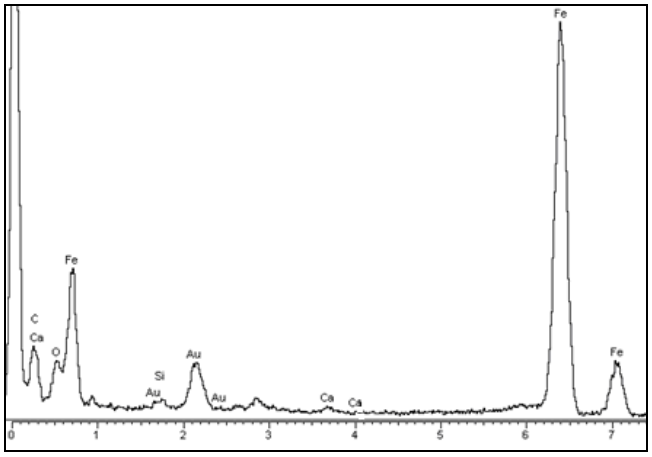

Figure 4: Typical EDS spectrum of an oxide film formed in the chloride-free solution (CH-0) obtained at the midpoint through the film.

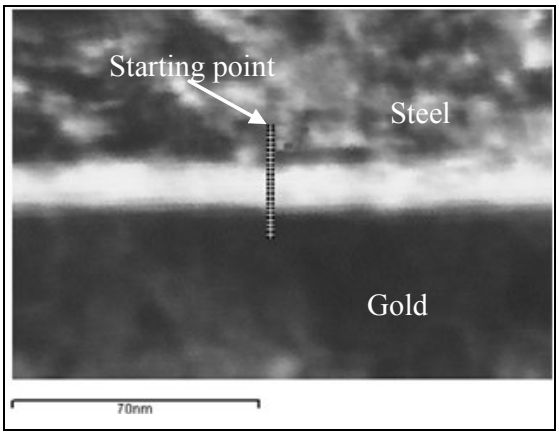

(a)

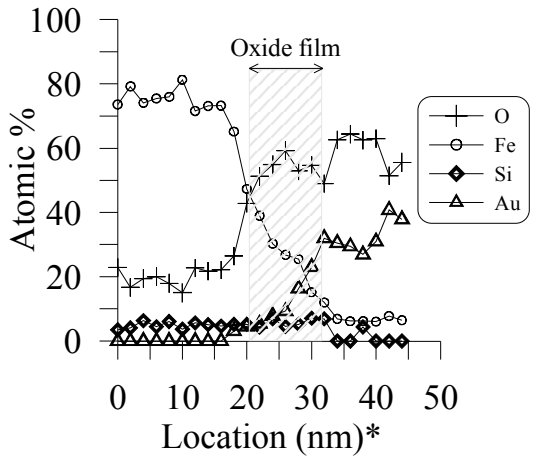

* Distance form the starting point shown in Fig. 5(a)

(b)

Figure 5: EDS analyses conducted on the CH-0 sample across the oxide film perpendicular to the steel surface: (a) TEM image showing the locations of the analyses; (b) EDS results corresponding to the points shown in the TEM image.

Additional evidence on the nature of the oxide film was obtained from dark-field TEM images. A dark-field TEM image taken of the oxide on the CH-0 sample is presented in Fig. 8. The bright phases, which are as large as 8 nm, are crystalline particles that compose the nanostructure of the oxide film.

4 CONCLUSIONS

The oxide films were 5 to 8 nm thick on rebar immersed for 15 days in chloride-free saturated calcium hydroxide 'simulated concrete pore' solution. Oxide films were mainly composed of nano-crystalline particles in various sizes up to 8 nm. After exposure to chloride in amounts larger than depassivation thresholds, iron oxides on the steel were no longer uniform and the average thickness of the oxide film was smaller than that observed before chloride exposure. In addition, some pit initiation sites were observed on the surface of steel.

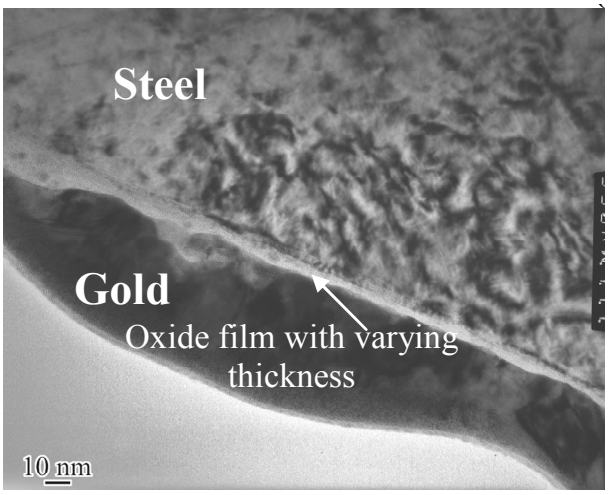

(a)

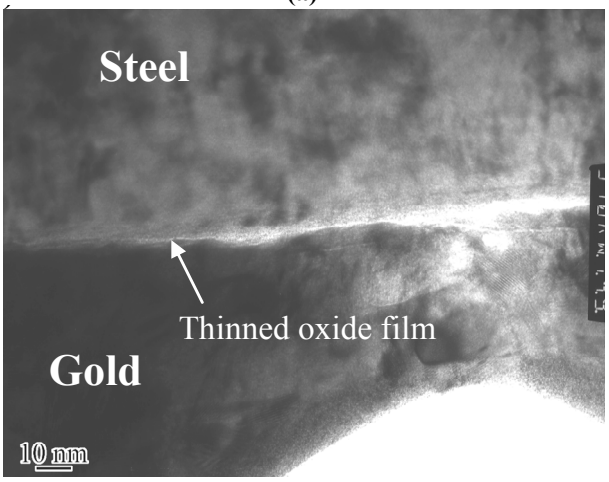

(b)

Figure 6: Typical TEM images of the oxide film from different parts of the CH-Cl sample showing: (a) non-uniform oxide thickness; (b) thinned oxide film.

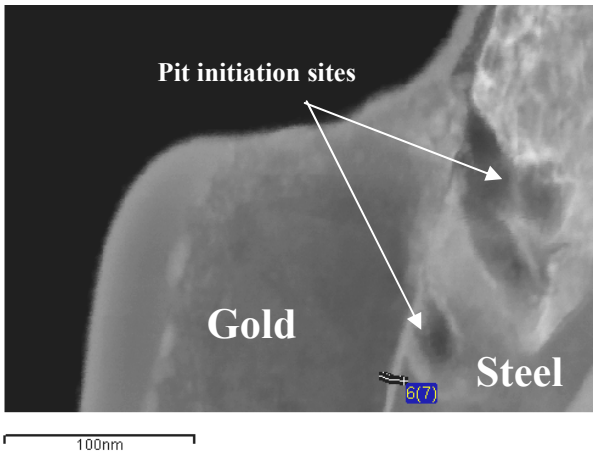

Figure 7: An TEM image of the CH-Cl sample showing two pits.

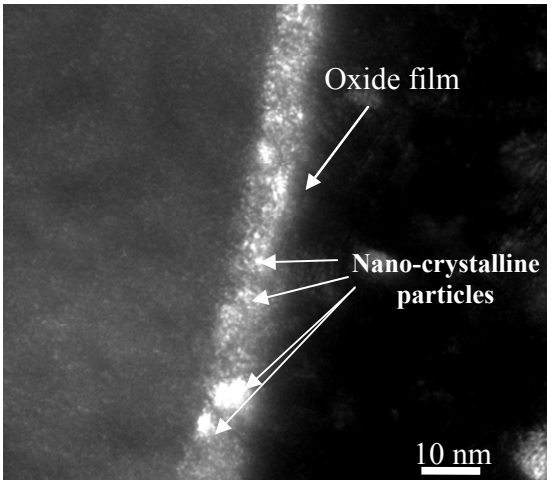

Figure 8: TEM dark-field image of the oxide film on the CH-0 sample.

ACKNOWLEDGMENTS

We would like to thank Ms. Catherine Bibby for her skilled assistance in the TEM investigation. This research was supported by a grant from the Natural Sciences and Engineering Research Council (NSERC) of Canada along with technical and financial support of CANMET-MTL laboratories, through the Resource for Innovation of Engineered Materials program. Both contributions are gratefully acknowledged.

REFERENCES

[1] L. F.Lin, C. Y.Chao and D. D. Macdonald, Journal of the Electrochemical Society, 128, 1194, 1981.
[2] J. Kruger, USA-Japan Seminar, NACE, Houston TX, 91, 1976.
[3] M. G. Alvarez and J. R. Galvele, Corrosion Science, 24, 1, 27, 1984.
[4] T. Zakroczymski, C. J. Fan and Z. Szklarska-Smialowska, Journal of the Electrochemical Society, 132, 2862, 1985.
[5] J. M. Sarver and Z. Szklarska-Smialowska, Localized Corrosion: Proceedings of an International Symposium Honoring Professor Marcel Pourbaix, 84, 328, 1984.
[6] S. Joiret, M. Keddam, X. R. Nóvoa, M. C. Pérez, C. Rangel and H. Takenouti, Cement and Concrete Composites, 24, 1, 75, 2002.
[7] P. Schmuki, M. Büchler, S. Virtanen, H. S. Isaacs, M. P. Ryan, and H. Böhni, Journal of the Electrochemical Society, 146, 6 , 2097, 1999.
[8] P. Ghods, O. B. Isgor, G. McRae and T. Miller, Cement and Concrete Composites, 31, 1, 2, 2009.
[9] P. Ghods, O. B. Isgor, G. A. McRae and G. P. Gu, Corrosion Science, doi:10.1016/j.corsci.2010.02.016.